Simulation of three-dimensional free-surface dam-break flows over a cuboid, cylinder, and sphere

Zhihua Xie[1], Thorsten Stoesser[2], and Junqiang Xia[3]

[1]Senior Lecturer, School of Engineering, Cardiff University, Cardiff, CF24 3AA, UK. E-mail: zxie@cardiff.ac.uk

[2]Professor, Department of Civil, Environmental and Geomatic Engineering, University College London, WC1E 6DE, UK. Email: t.stoesser@ucl.ac.uk

[3]Professor, State Key Laboratory of Water Resources and Hydropower Engineering Science, Wuhan University, Wuhan 430072, China. Email: xiajq@whu.edu.cn

ABSTRACT

A three-dimensional (3D) numerical study has been undertaken to investigate dam-break flows over 3D structures. A two-phase flow model has been developed within the large-eddy simulation (LES) framework. The governing equations have been discretised using the finite volume method, with the air-water interface being captured using a volume-of-fluid method whilst the Cartesian cut-cell method deals with complex geometries. The robustness and versatility of the proposed numerical approach are demonstrated first by applying it to a 3D dam-break flow over a cuboid. Good agreement is obtained between the simulation results and the corresponding experimental data and other numerical solutions. Then, a horizontal cylinder and a sphere are subjected to the same dam-break flow. Snapshots of water surface profiles are presented and discussed and turbulent vortical structures are identified in the flow. In addition, the pressure distribution around the structure, velocity field on the air-water interface, hydrodynamic loading on the structure, and energy dissipation during dam-break flow impact are analysed and discussed, providing more insight into such flows.

INTRODUCTION

Dam-break flows are an important phenomenon appearing in civil engineering applications potentially leading to severe flooding of communities downstream of the dam with catastrophic consequences, such as damage to buildings and infrastructure and loss of human life, such as the recent Michigan dam failure in May 2020. The hydraulics of dam-break flows (Costa and Schuster 1988) is affected by the mode of dam failure and how the failure propagates as a function of time, as well as its underlying complex topography and the presence of structures in its path. Dam-break flow interacting with structures results in complex three-dimensional (3D) hydrodynamics and substantial turbulence. In the past, significant advances have been made based on theoretical (Stoker 1957), experimental (Martin and Moyce 1952; Stansby et al. 1998; Janosi et al. 2004; Soares-Frazao and Zech 2008) and numerical studies of dam-break flows (Toro and Garcia-Navarro 2007). An ability to predict accurately the complex fluid-structure interaction of dam-break flows enables a better understanding of the resulting inundation and the structural response of buildings in a dam-break flows path.

Much effort has been devoted to develop numerical methods for dam-break flows. Commonly used are one-dimensional (1D) or two-dimensional (2D) depth-averaged shallow water equation (SWE) models, respectively and have been applied to simplified (Liang et al. 2006; Wu and Wang 2007) or realistic (Sleigh et al. 1998; Zhou et al. 2004; Liang and Borthwick 2009; Kesserwani and Liang 2010; Xia et al. 2010) domains, predicting fairly accurately flood inundation and horizontal velocities. Due to the assumption of hydrostatic pressure and depth-averaging of the velocity, SWE models are unable to provide the detailed near-field flow, and thus loadings and stresses around a structure immersed in a dam-break flow.

Continuous development of Computational Fluid Dynamics (CFD) methods and accompanied by constant increase in computer power have facilitated solving the Navier-Stokes equations (NSE) together with free surface calculations (McSherry et al. 2017). Various methods for dam-break flows have been developed for predicting the NSE together with the volume-of-fluid method on fixed (Lin and Xu 2006; Kleefsman et al. 2005) or adaptive (Greaves 2006; Pavlidis et al. 2016)

grids, the level set method (Yue et al. 2003), the smooth particle hydrodynamics (SPH) method (Shao and Lo 2003; Gomez-Gesteira and Dalrymple 2004), and the non-hydrostatic model (Ai et al. 2011). In order to deal with complex topography and structures, body-fitted (Stoesser et al. 2008) or unstructured grid (Pavlidis et al. 2016) and Cartesian grid method (Mittal and Iaccarino 2005; Kara et al. 2015; Xie and Stoesser 2020a) can be used. Most dam-break flows and their interaction with surrounding structures are turbulent, and therefore the effect of turbulence on the mean and instantaneous flows needs to be considered unless all scales of turbulence are fully resolved. In the past, the turbulence effect has been considered in several 3D dam-break flows based on the Reynolds-averaged Navier–Stokes (RANS) equations (Yang et al. 2010; Marsooli and Wu 2014; Munoz and Constantinescu 2020) or large-eddy simulation (LES) (Wu 2004; Wei et al. 2015) for uneven beds or vertical structures (such as bridge piers or buildings).

Many SWE and 3D NSE models suffer from numerical instabilities near the free surface (Kleefsman et al. 2005) which can be overcome by two-phase flow models, in which the air and water phase are solved simultaneously. Such models have been employed for breaking waves (Xie 2012) and wave-structure interaction (Xie et al. 2020). When there is significant fluid-structure interaction (FSI), air entrainment (Kiger and Duncan 2012) can become important, hence the adoption of a two-phase flow model for FSI is preferred.

The objective of this study is therefore, to refine and validate a two-phase flow model (Xie 2012; Xie 2015) using the newly developed Cartesian cut-cell method (Xie and Stoesser 2020a) and to perform large-eddy simulations of 3D dam-break flows with complex structures with the aim to predict accurately various quantities for dam-break flows impact on structures, such as water surface elevations, water surface profiles, hydrodynamic loading on structures, and energy dissipation at high temporal and spatial resolution.

NUMERICAL FRAMEWORK

The in-house LES code (Xdolphin3D) (Xie 2012; Xie 2015; Xie and Stoesser 2020a) is employed in this study. The code solves the filtered Navier-Stokes equations on a staggered Cartesian grid based on the finite volume method and the dynamic Smagorinsky subgrid-scale

model is employed to compute the unresolved scales of turbulence. A first-order or second-order backward Euler method is used for the time derivative, which leads to an implicit scheme for the Navier-Stokes equations and the PISO algorithm (Issa 1986) is employed for the pressure-velocity coupling. In order to combine high-order accuracy with monotonicity, the advection terms are discretised by a high-resolution scheme (Xie 2012), whereas central difference schemes are used for the diffusion and pressure terms. In order to deal with complex geometries in Cartesian grids, the 3D cut-cell method developed by Xie and Stoesser (2020a) is utilised in the finite volume discretisation. Special treatment is needed in cut cells, for the advective and diffusive fluxes at cell faces, as well as cell volumes. The high-resolution VOF scheme CICSAM (Compressive Interface Capturing Scheme for Arbitrary Meshes) (Ubbink 1997) is used to capture the air-water interface, which is defined as the volume fraction is equal to 0.5. The two-phase flow code has already been extensively benchmarked and validated through a series of test cases for breaking waves (Xie 2012; Xie 2015; Xie and Stoesser 2020b), LES studies of open-channel and free-surface flows over rough beds (Xie et al. 2013a; Xie et al. 2013b; Xie et al. 2014; Xie et al. 2021) and moving bodies (Xie and Stoesser 2020a), and wave-structure interaction (Xie et al. 2020).

RESULTS AND DISCUSSION

In this section, the results of dam-break flow simulations over a cuboid are presented first with the goal to validate the present numerical approach. Once validated successfully a circular cylinder and a sphere are subjected to the same dam-break flows with the goal to expand current knowledge of dam-break-flow-structure interaction. Finally, the key parameters (hydrodynamic loads, energy dissipation and mass conservation) are compared between three different structures subjected to dam-break flows.

Dam-break flow over a cuboid

A dam-break flow over a cuboid, for which an experiment was carried out in the Maritime Research Institute Netherlands (MARIN) (Kleefsman et al. 2005) is considered. The time history of both the water surface elevation at several locations and the pressure on the cuboid were measured in the experiment.

The LES is set up to replicate the laboratory tank, which was 3.22 m long, 1 m high and 1 m wide (as shown in Fig. 1). A rectangular cuboid of $0.161(\mathrm{m}) \times 0.161(\mathrm{m}) \times 0.403(\mathrm{m})$ is placed downstream of a water column with its initial height at 0.55 m. Two water surface gauges at the front and back of the releasing gate, and four pressure transducers at the front and the top of the cuboid are implemented during the simulation to sample numerical data that can be compared to the experimental measurements. A uniform mesh $322 \times 100 \times 100$ is used and the total number of cells is 3.22 million. The velocity field is initialised as zero for both air and water with a hydostatic pressure and an adaptive time step with a maximum CFL number 0.2 is used in the simulation.

Fig. 2 shows snapshot of the predicted water surface profiles after the collapse of the water column, together with the experimental measurement and the single-phase VOF model of Kleefsman et al. (2005). It is shown that the water starts to collapse due to gravity and is almost two-dimensional before it hits the box. A jet is formed at the front face of the box during the impact, moving upwards and a little bit forward, whereas both sides wrap around the box and move towards the tank end. The two leading edges impacts on the tank wall and move upwards and towards the centre. Some of the water start to fall down on the wall due to gravity and some of the leading edges collide at the centre to form a thin sheet moving back towards the obstacle. After impact, the water flows back to the reservoir and complex air entrainment can be observed. It can be seen from Fig. 2 that a good agreement is obtained between the snapshots of the present two-phase flow simulation and the experiment as well as the single-phase flow model from Kleefsman et al. (2005).

In order to make quantitative comparison, the time histories of the water height at gauges H4 and H2 are compared with the experimental data and the single-phase flow model from Kleefsman et al. (2005) in Fig. 3. Overall, both numerically obtained water heights agree reasonably well with the experimental data. The mean absolute percentage errors between the present and experimental results for gauges H4 and H2 are 4% and 7%, respectively. Slight discrepancies between measurement and simulation at a later stage is observed at H2, which can be attributed to the complex wave impact. Some phase difference can be observed and the wave propagation speed is not well captured which might be partly due to the unresolved bed friction in the turbulent boundary layer,

and partly due to smaller air-bubbles being entrained into the flow not being captured with the present mesh resolution.

Time history of the computed pressure as well as the measured and simulated pressure from Kleefsman et al. (2005) at the front and top faces of the obstacle are plotted in Fig. 4. Generally, convincing agreement between the two-phase flow simulation and experiment is obtained during initial impact at the front face (P1 and P3). The peak pressure is well captured and the return wave (around $t = 5$ s) can also be noticed although there is a phase shift as mentioned above. On the top of the obstacle (P5 and P7), there are some oscillation for the pressure which is due to the complex wave impact shown in Fig. 2. Overall, it can be observed that better agreement with the experiment for the pressure field is obtained for the present two-phase flow approach, and there are no large spurious spikes which are often observed in singe-phase flow models as seen in Fig. 4 and also Fig.11 in Marsooli and Wu (2014). Kleefsman et al. (2005) discussed that interpolation is needed to get values in surface cells in the single-phase flow model, these spikes are caused by the surface (or empty) cell changes to a fluid cell which the divergence is not zero. However, in the present two-phase flow model, both air and water are solved and the divergence free is ensured for all the cells in the computational domain and hence eliminates such pressure spikes.

Dam-break flow over a horizontal cylinder

In this section, a horizontal circular cylinder is subjected to a dam-break flow, which is often observed in large woody debris dams for natural flood reduction and coastal flooding over pipelines. This kind of flow is different from the commonly used vertical cylinder and this case can not be studied by employing 2D SWE models. The computational setup and mesh is the same as that used in the previous section, only the cuboid is replaced by a circular cylinder with the same height and width as the cuboid (shown in Fig. 1).

Fig. 5 shows snapshots of the predicted water surface profiles during dam-break flow impact. Compared to the cuboid case, it can be seen that a curved jet (at $t = 0.56$ s) is formed when the water hits the cylinder due to the curvature of the surface. The jet overtops the cylinder with much lower height than previous case, but moves further towards the tank wall. As a consequence, less

water comes around either side of the obstacle and the impact velocity for the leading edges is smaller as observed from the height on the wall (at $t = 0.8$ s). After that ($t = 1.2 - 2.0$ s), the water is reflected and returns back towards the reservoir with a similar pattern shown in Fig. 2. For different geometry of the structures under the same dam-break flow, it is shown that the wave impact is weaker for the circular cylinder case, which is due to the round edge during fluid-structure interaction.

Fig. 6 shows water surface profiles and the streamwise velocity u along the central plane. At the initial impact (at $t = 0.56$ s), the water surface profiles are similar for both cases whereas they are significantly different in the vicinity of the structure. The streamwise velocity u is higher for the cylinder case while the vertical velocity is higher for the cuboid case as the the jet is higher. In front of the structure near the bed, the flow is reflected and it can be observed that the sign of the streamwise velocity changes there. At $t = 0.8$ s, the jet moves faster for the cylinder case with its height lower than the cuboid case. As more water pass by the cuboid (at $t = 1.2$ s), the reflected velocity from the end wall is higher and the enclosed cavity is larger beneath the jet. When the reflected wave returns to the structure (at $t = 2.0$ s), complex air-water interfaces can be observed for both cases with air entrainment phenomena. The air cavity breaks up and a large number of bubbles are formed when the reflected wave hits the structure. At this stage, the air-water interface is unstable and has multiple length scales affected by the surface tension, turbulence and mean flow. It can be seen from Fig. 2 and Fig. 5 that less bubbles entrained in the water and less droplets are obtained for the cylinder case. It is worth noting that the two-phase flow model is useful to study the detailed air entrainment phenomena. The air entrainment considered here is less significant compared to dam spillways (white water phenomenon), which will require very fine spatial resolution to capture the formulation and transport of a wide range of small bubbles and their size distribution and is beyond the scope of this study.

Dam-break flow over a sphere

The computational setup and mesh are the same as the ones reported in the previous two sections, with a sphere of similar cross sectional area (radius $r = 0.15$ m) to both the cuboid and

the cylinder is placed at the same location as before and subjected to the same dam-break flow as shown in Fig. 1.

Fig. 7 shows the predicted water surface evolution and associated turbulent vortical structures, which is plotted via isosurfaces of λ_2 (the second invariant of the velocity gradient tensor (Jeong and Hussain 1995)), to identify vortex cores. Both oblique and top views are presented in order to appreciate the complex 3D flow and turbulent structures. During initial impact (t = 0.56 s), there is a pair of counter-rotating vortices developed in front of the sphere, as the flow is diverted by the sphere. Large vortical structures are also observed in the vicinity of the air-water interface, with opposite signs on either side of the sphere. At later stage (t = 0.8 s), two leading edges of the flow hit the end of the tank and the water starts to overtop the sphere at lower water depth than for the cuboid (Fig. 2) and the cylinder (Fig. 5) flows. At t = 1.2 s, the pair of counter-rotating vortices in front of the sphere becomes weaker and moves a little bit backwards. When the wave is reflected back from the end wall (t = 2.0 s), complex jet impingement and air entrainment can be observed, associated with much stronger turbulent vortical structures both in the water and near the air-water interface.

Comparison between 3D structures

Accurate prediction of hydrodynamic loads will lead to better understanding of the risk assessment of infrastructure during dam-break flow and flooding events. The drag coefficient obtained from the 3D model is useful to account for local losses due to 3D structures in depth-averaged models. For different 3D structures, the hydrodynamic loads are normalised by the cross section area in order to make comparison in the present study.

Fig. 8 shows the computed drag F_x (left) and lift F_y (right) forces on the three different structures during the simulation. The forces increase suddenly when the water hits the structures and have a local maximum at the initial stage. The horizontal force changes direction when the reflected wave impacts on the structures (around t = 1.5 s), and remains in the positive streamwise direction until the moment of the return flow hits the structures again (around t = 5 s). Compared to the three cases, the cuboid has the highest horizontal force at the initial impact whereas the sphere

has the highest value when the first wave returned to the structures. The maximum force for the sphere is higher during the reflected flow than the initial impact. Overall, the cuboid has the highest horizontal force during the dam-break flow, and the maximum force is approximately 93% and 33% of that value for the cylinder and sphere, respectively.

For the vertical force, the curved surface (cylinder and sphere) always has a positive value during the whole simulation as the flow attempts to lift these structures up. The negative vertical force only occurs for the cuboid case when the returned flow hits the structure. Compared to the three cases, the cylinder has the highest vertical force at the initial impact whereas the sphere has the highest value at later stage. It is worth noting that the cuboid and sphere have similar maximum vertical force during the initial impact, which is approximately 18% of the value for the cylinder case.

In order to study the energy dissipation mechanism and mass conservation for the complex two-phase flow during dam-break flow impact, the time history of the kinetic, potential, total energy, and total mass are shown in Fig. 9, where the energy is calculated by integrating the region in the water for the whole computational domain and normalised by the initial total energy. When the water in the reservoir collapses, the potential energy decreases and transfers into the kinetic energy. The kinetic energy achieves its maximum value during the flow impact on the structures whereas the potential energy has a local minimum. The kinetic energy starts to decrease when the flow passes over the structures and transfers some part back into the potential energy. There are some fluctuation of the kinetic and potential energy at later stage and eventually the kinetic energy will reduce to zero with potential energy converged to a certain value when the air-water interface becomes flat. There is stronger energy dissipation from $t = 0-2$ s, which is mainly attributed to the vorticity and turbulence generation during complex turbulent two-phase flows. During this time, the sphere has the highest kinetic energy whereas the potential energy fluctuates between the three cases. Overall, the total energy dissipation is highest for the cuboid case while it is lowest for the sphere case which is due to the lower drag and lift forces. It is worth mentioning that comparison for the energy dissipation is only for present computational setup with the same initial stage of

dam-break flows and similar volume of the structures. Different flow regime and different size of structures might affect the energy dissipation, which is beyond the scope of this study.

Finally, mass conservation of the complex dam-break flow impact simulations is computed, and it is found that the errors of the total mass during the simulations are less than 0.3% for all cases considered here (shown in the last plot of Fig. 9), indicating a good mass conservation being achieved for the present two-phase flow code.

CONCLUSION

In this study, a LES-based two-phase flow code Xdolphin3D has been introduced able to predict 3D dam-break flow-structure interaction. Different complex structures are well represented by the Cartesian cut-cell method. Simulations of dam-break flow over cuboid have been qualitatively and quantitatively compared with experimental measurements, with better agreement being obtained from the present two-phase LES model and there are no large spurious spikes for pressure which are often observed in single-phase flow models.

The free-surface flows during dam-break over a cuboid, cylinder, and sphere are presented in detail, demonstrating the fully 3D flow field, which is difficult to study in SWE models. The shape of the structures with similar volume has a significant effect on the free-surface flow field for the same incoming dam-break flow, which in return will change the hydrodynamic loadings and stresses around the structures. Different from single-phase flow over structures, it is found that the hydrodynamic load changes with time regarding the dam-break flows and the cuboid has the maximum drag force whereas the cylinder has the maximum lift force. Complex vortical structures and air entrainment are generated during flow-structure interaction, which change the energy dissipation associated with the flow.

DATA AVAILABILITY STATEMENT

Some or all data, models, or code that support the findings of this study are available from the corresponding author upon reasonable request (numerical results and flow profiles).

ACKNOWLEDGEMENTS

Financial support was provided by the Royal Society Newton Advanced Fellowship (NAF/R1/201156), the EPSRC grants (EP/R022135/1 and EP/S016376/1), and Cardiff University GCRF project. Constructive comments from anonymous reviewers and the Associate Editor for the improvement of the manuscript are gratefully acknowledged.

REFERENCES

Ai, C., Jin, S., and Lv, B. (2011). "A new fully non-hydrostatic 3d free surface flow model for water wave motions." *International Journal for Numerical Methods in Fluids*, 66(11), 1354–1370.

Costa, J. and Schuster, R. (1988). "The formation and failure of natural dams." *Geological Society of America Bulletin*, 100(7), 1054–1068.

Gomez-Gesteira, M. and Dalrymple, R. A. (2004). "Using a three-dimensional smoothed particle hydrodynamics method for wave impact on a tall structure." *Journal of Waterway, Port, Coastal, and Ocean Engineering*, 130(2), 63–69.

Greaves, D. M. (2006). "Simulation of viscous water column collapse using adapting hierarchical grids." *International Journal for Numerical Methods in Fluids*, 50(6), 693–711.

Issa, R. I. (1986). "Solution of the implicitly discretised fluid flow equations by operator-splitting." *Journal of Computational Physics*, 62(1), 40–65.

Janosi, I. M., Jan, D., Szabo, K. G., and Tel, T. (2004). "Turbulent drag reduction in dam-break flows." *Experiments in Fluids*, 37, 219–229.

Jeong, J. and Hussain, F. (1995). "On the identification of a vortex." *Journal of Fluid Mechanics*, 285, 69–94.

Kara, S., Kara, M. C., Stoesser, T., and Sturm, T. W. (2015). "Free-surface versus rigid-lid les computations for bridge-abutment flow." *Journal of Hydraulic Engineering*, 141(9), 04015019.

Kesserwani, G. and Liang, Q. (2010). "A discontinuous galerkin algorithm for the two-dimensional shallow water equations." *Computer Methods in Applied Mechanics and Engineering*, 199(49), 3356 – 3368.

Kiger, K. T. and Duncan, J. H. (2012). "Air-entrainment mechanisms in plunging jets and breaking waves." *Annual Review of Fluid Mechanics*, 44, 563–596.

Kleefsman, K. M. T., Fekken, G., Veldman, A. E. P., Iwanowski, B., and Buchner, B. (2005). "A volume-of-fluid based simulation method for wave impact problems." *Journal of Computational Physics*, 206(1), 363–393.

Liang, D., Falconer, R. A., and Lin, B. (2006). "Comparison between TVD-MacCormack and ADI-type solvers of the shallow water equations." *Advances in Water Resources*, 29(12), 1833 – 1845.

Liang, Q. and Borthwick, A. G. (2009). "Adaptive quadtree simulation of shallow flows with wet-dry fronts over complex topography." *Computers & Fluids*, 38(2), 221 – 234.

Lin, P. and Xu, W. (2006). "NEWFLUME: a numerical water flume for two-dimensional turbulent free surface flows." *Journal of Hydraulic Research*, 44, 79–93.

Marsooli, R. and Wu, W. (2014). "3-d finite-volume model of dam-break flow over uneven beds based on vof method." *Advances in Water Resources*, 70, 104 – 117.

Martin, J. C. and Moyce, W. J. (1952). "An experimental study of the collapse of liquid columns on a rigid horizontal plane .4.." *Philosophical Transactions of the Royal Society of London Series a-Mathematical and Physical Sciences*, 244(882), 312–324.

McSherry, R., Chua, K. V., and Stoesser, T. (2017). "Large eddy simulation of free-surface flows." *Journal of Hydrodynamics, Ser. B*, 29, 1–12.

Mittal, R. and Iaccarino, G. (2005). "Immersed boundary methods." *Annual Review of Fluid Mechanics*, 37, 239–261.

Munoz, D. H. and Constantinescu, G. (2020). "3-d dam break flow simulations in simplified and complex domains." *Advances in Water Resources*, 137, 103510.

Pavlidis, D., Gomes, J. L. M. A., Xie, Z., Percival, J. R., Pain, C. C., and Matar, O. K. (2016). "Compressive advection and multi-component methods for interface-capturing." *International Journal of Numerical Methods in Fluids*, 80, 256–282.

Shao, S. and Lo, E. Y. (2003). "Incompressible sph method for simulating newtonian and non-

newtonian flows with a free surface." *Advances in Water Resources*, 26(7), 787 – 800.

Sleigh, P., Gaskell, P., Berzins, M., and Wright, N. (1998). "An unstructured finite-volume algorithm for predicting flow in rivers and estuaries." *Computers and Fluids*, 27(4), 479 – 508.

Soares-Frazao, S. and Zech, Y. (2008). "Dam-break flow through an idealised city." *Journal of Hydraulic Research*, 46, 648–658.

Stansby, P. K., Chegini, A., and Barnes, T. C. D. (1998). "The initial stages of dam-break flow." *Journal of Fluid Mechanics*, 374, 407424.

Stoesser, T., Braun, C., Garcia-Villalba, M., and Rodi, W. (2008). "Turbulence structures in flow over two-dimensional dunes." *J. Hydraul. Eng.*, 134(1), 42–55.

Stoker, J. (1957). *Water waves*. Interscience Publishers, New York.

Toro, E. F. and Garcia-Navarro, P. (2007). "Godunov-type methods for free-surface shallow flows: A review." *Journal of Hydraulic Research*, 45(6), 736–751.

Ubbink, O. (1997). "Numerical prediction of two fluid systems with sharp interfaces." Ph.D. thesis, Imperial College of Science, Technology and Medicine, London, UK.

Wei, Z., Dalrymple, R. A., Hérault, A., Bilotta, G., Rustico, E., and Yeh, H. (2015). "Sph modeling of dynamic impact of tsunami bore on bridge piers." *Coastal Engineering*, 104, 26 – 42.

Wu, T. R. (2004). "A numerical study of three-dimensional breaking waves and turbulence effects." Ph.D. thesis, Cornell University, US.

Wu, W. and Wang, S. S. (2007). "One-dimensional modeling of dam-break flow over movable beds." *Journal of Hydraulic Engineering*, 133(1), 48–58.

Xia, J., Lin, B., Falconer, R. A., and Wang, G. (2010). "Modelling dam-break flows over mobile beds using a 2d coupled approach." *Advances in Water Resources*, 33(2), 171 – 183.

Xie, Z. (2012). "Numerical study of breaking waves by a two-phase flow model." *Int. J. Numer. Meth. Fluids*, 70(2), 246–268.

Xie, Z. (2015). "A two-phase flow model for three-dimensional breaking waves over complex topography." *Proc. R. Soc. A*, 471, 20150101.

Xie, Z., Lin, B., Falconer, R., Nichols, A.N. Tait, S., and Horoshenkov, K. (2021). "Large-eddy

simulation of turbulent free surface flow over a gravel bed." *Journal of Hydraulic Research* , accepted.

Xie, Z., Lin, B., and Falconer, R. A. (2013a). "Large-eddy simulation of the turbulent structure in compound open-channel flows." *Adv. Water Res.*, 53, 66–75.

Xie, Z., Lin, B., and Falconer, R. A. (2014). "Turbulence characteristics in free-surface flow over two-dimensional dunes." *J. Hydro-Environ. Res.*, 8(3), 200–209.

Xie, Z., Lin, B., Falconer, R. A., and Maddux, T. B. (2013b). "Large-eddy simulation of turbulent open-channel flow over three-dimensional dunes." *J. Hydraul. Res.*, 51(5), 494–505.

Xie, Z. and Stoesser, T. (2020a). "A three-dimensional Cartesian cut-cell/volume-of-fluid method for two-phase flows with moving bodies." *Journal of Computational Physics*, 461, 109536.

Xie, Z. and Stoesser, T. (2020b). "Two-phase flow simulation of breaking solitary waves over surface-piercing and submerged conical structures." *Ocean Engineering*, 213, 107679.

Xie, Z., Stoesser, T., Yan, S., Ma, Q., and Lin, P. (2020). "A Cartesian cut-cell based multiphase flow model for large-eddy simulation of three-dimensional wave-structure interaction." *Computers and Fluids*, 213, 104747.

Yang, C., Lin, B., Jiang, C., and Liu, Y. (2010). "Predicting near-field dam-break flow and impact force using a 3d model." *Journal of Hydraulic Research*, 48, 784–792.

Yue, W., Lin, C. L., and Patel, V. C. (2003). "Numerical simulation of unsteady multidimensional free surface motions by level set method." *International Journal for Numerical Methods in Fluids*, 42, 853–884.

Zhou, J. G., Causon, D. M., Mingham, C. G., and Ingram, D. M. (2004). "Numerical prediction of dam-break flows in general geometries with complex bed topography." *Journal of Hydraulic Engineering*, 130(4), 332–340.

List of Figures

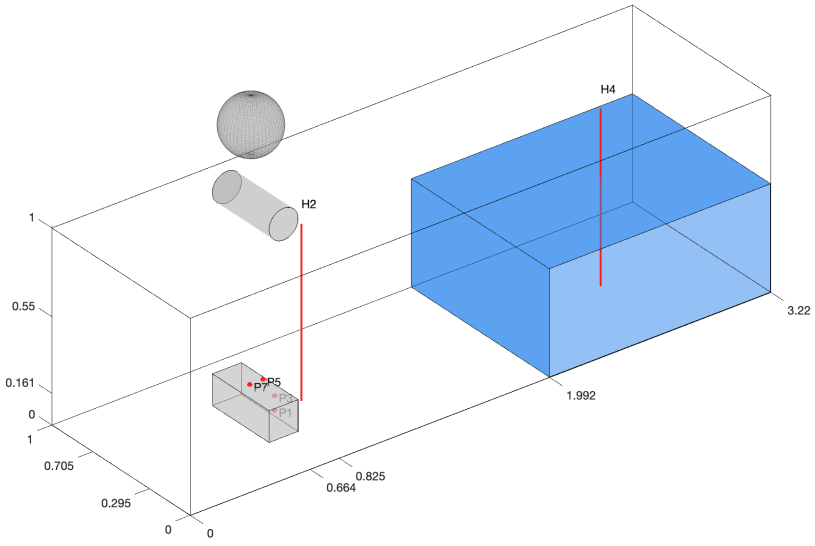

Fig. 1. Schematic of computational setup of a dam-break flow over a structure. Only the cuboid is placed in the tank and it will be replaced with the cylinder and sphere for different cases.

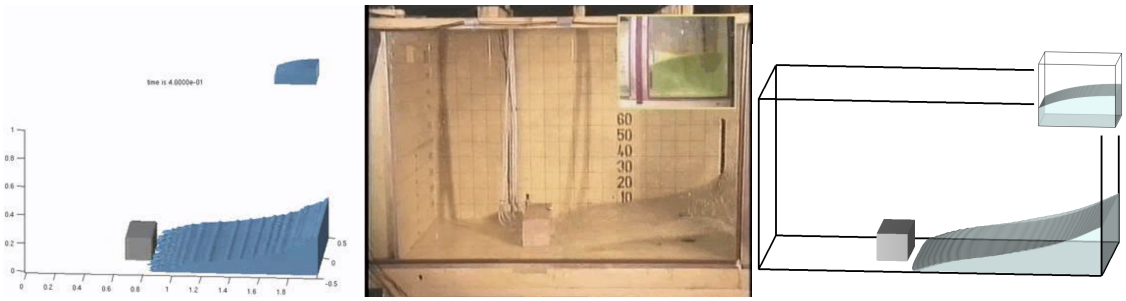

(a) $t = 0.4$ s

(b) $t = 0.56$ s

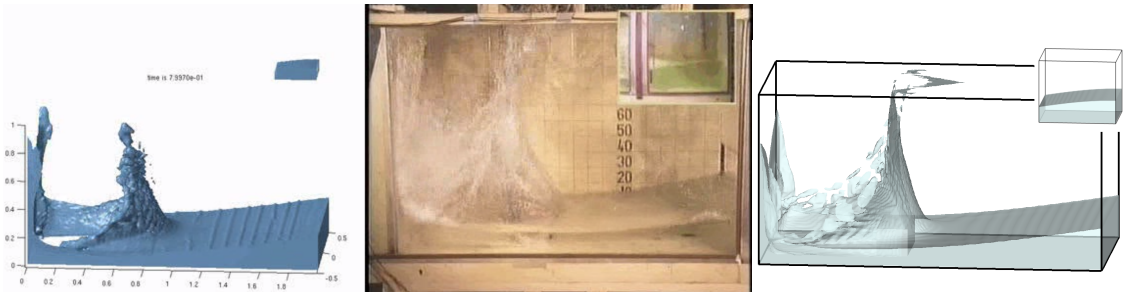

(c) $t = 0.8$ s

(d) $t = 1.2$ s

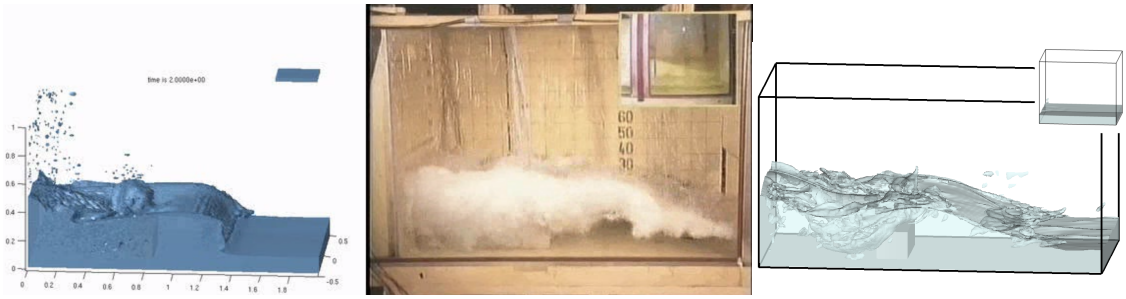

(e) $t = 2.0$ s

Fig. 2. Snapshots of the dam-break flows of the single-phase flow model (left), experiment (Kleefsman et al. 2005) (middle), and the present two-phase flow approach (right) at t (s) = 0.4 (a), 0.56 (b), 0.8 (c), 1.2 (d), and 2.0 (e). The smaller pictures on the top right inside the snapshots show the water in the reservoir. The water surfaces are shown as the isosurface of volume fraction $F = 0.5$ and the single-phase and experimental snapshots are obtained from http://www.math.rug.nl/~veldman/comflow/dambreak.html.

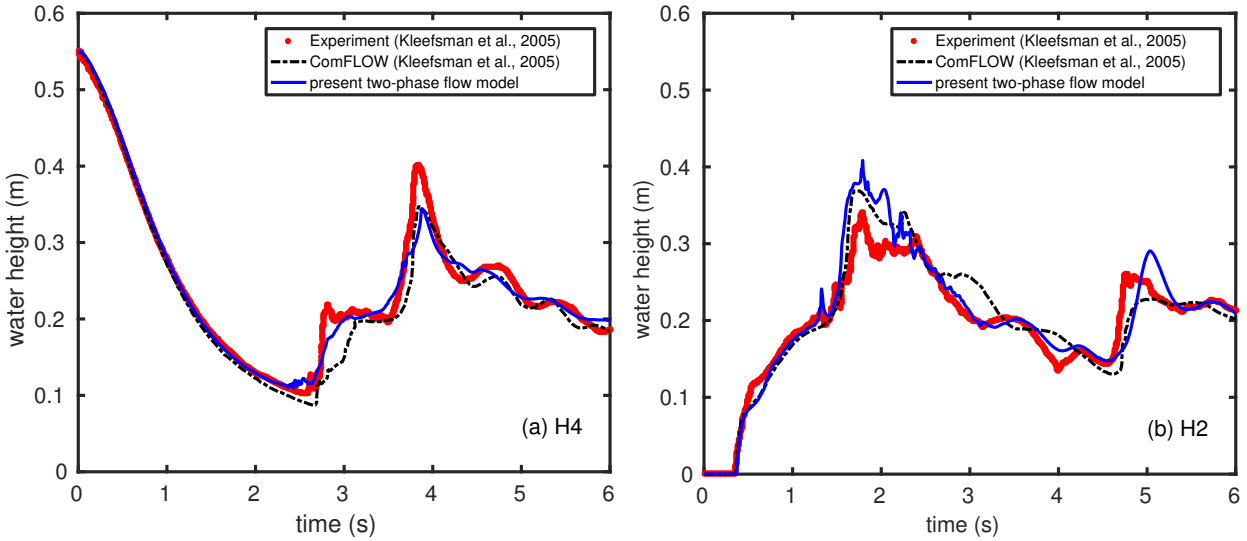

Fig. 3. Time history of the water height in the reservoir H4 (a) and in the tank H2 (b). Present two-phase VOF model results are compared with the experimental and single-phase VOF model results from Kleefsman et al. (2005).

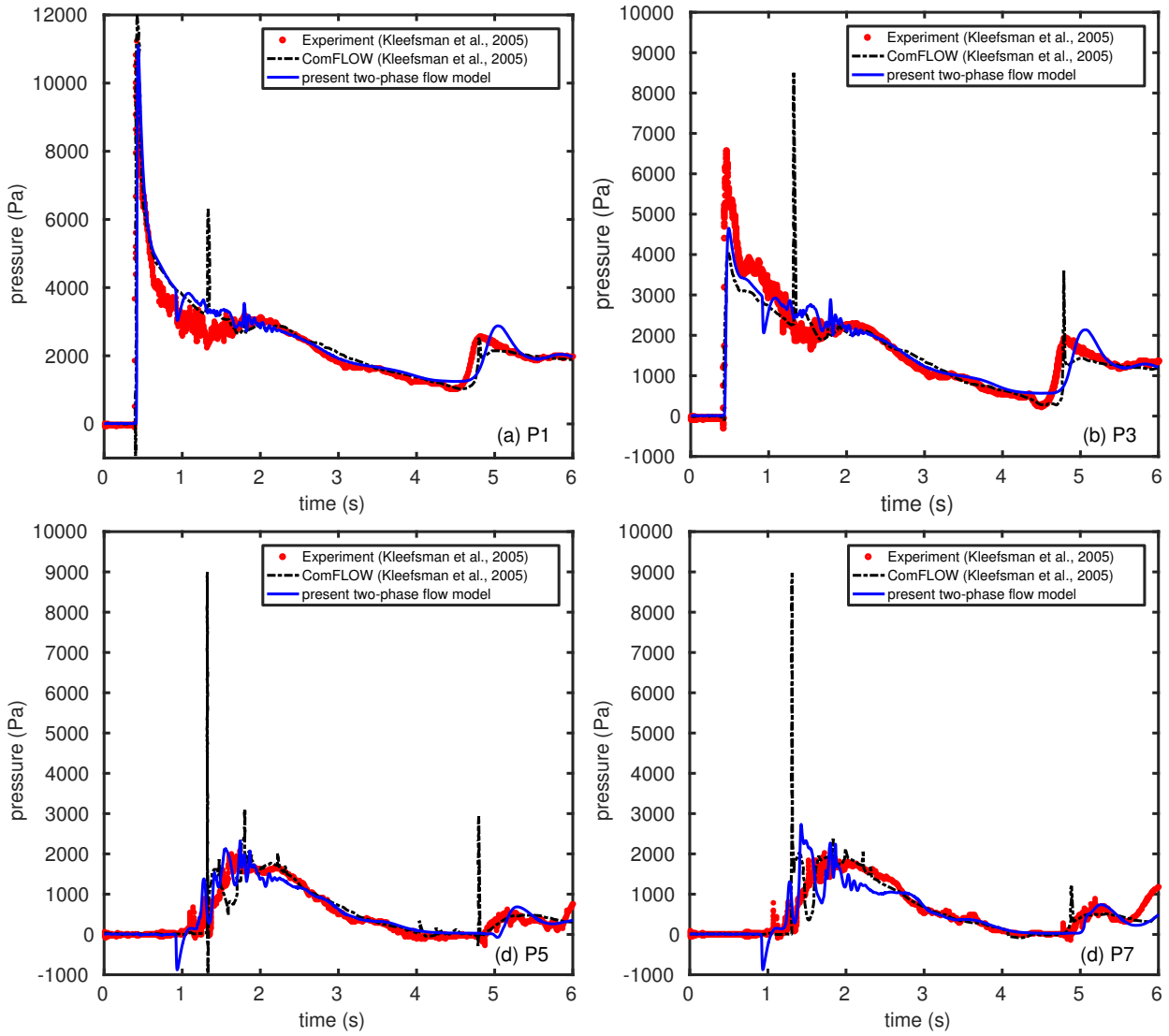

Fig. 4. Time history of the pressure at locations P1 (a), P3(b), P5(c) and P7 (d). Present two-phase VOF model results are compared with the experimental and single-phase VOF model results from Kleefsman et al. (2005).

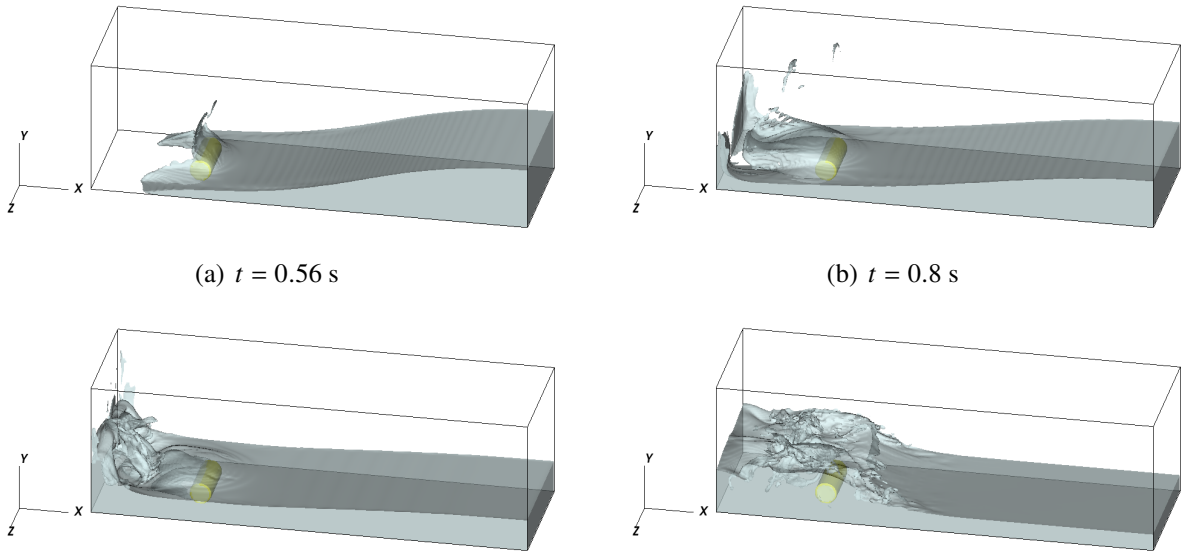

(a) t = 0.56 s (b) t = 0.8 s

(c) t = 1.2 s (d) t = 2.0 s

Fig. 5. Snapshots of the dam-break flow over a horizontal cylinder at t (s) = 0.56 (a), 0.8 (b), 1.2 (c), and 2.0 (d), where the water surfaces are shown as the isosurface of volume fraction F = 0.5.

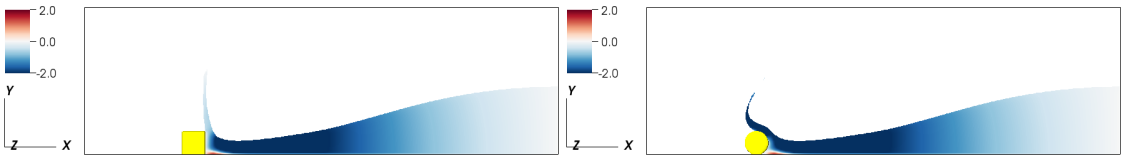

(a) t = 0.56 s

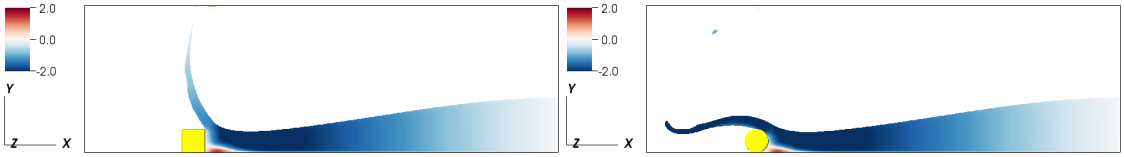

(b) t = 0.80 s

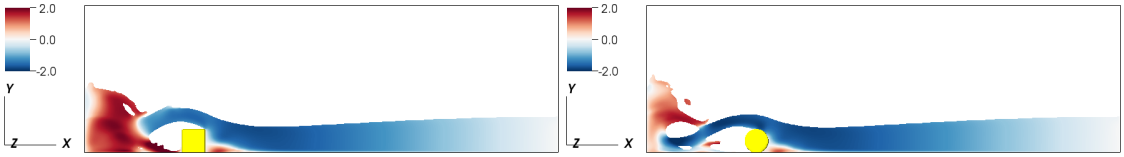

(c) t = 1.20 s

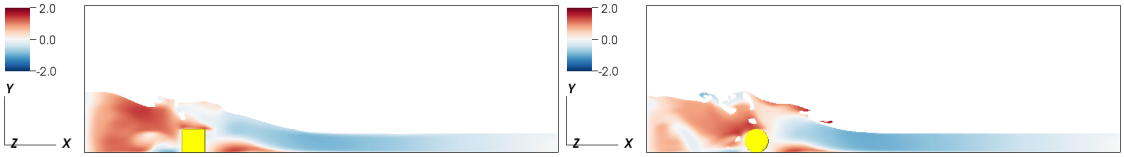

(d) t = 2.00 s

Fig. 6. Comparison of the water surface profiles between the cuboid (left) and cylinder (right) cases at t (s) = 0.56 (a), 0.8 (b), 1.2 (c), and 2.0 (d), where the water surface is colored by the streamwise velocity u.

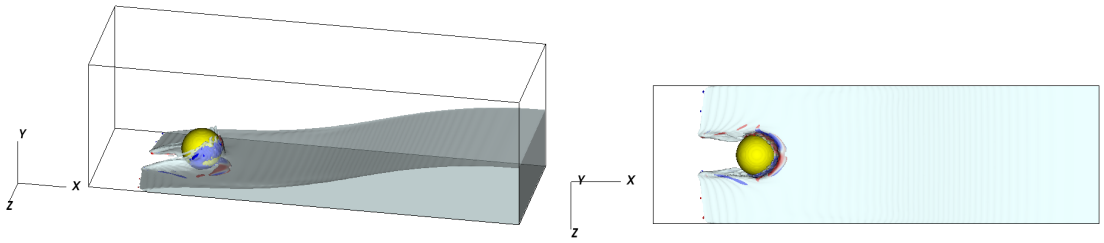

(a) t = 0.56 s

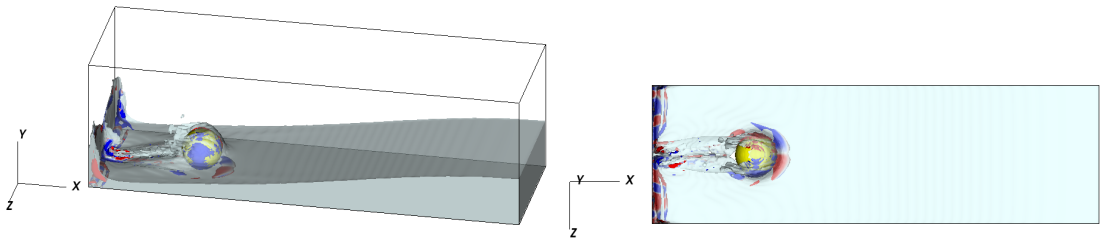

(b) t = 0.8 s

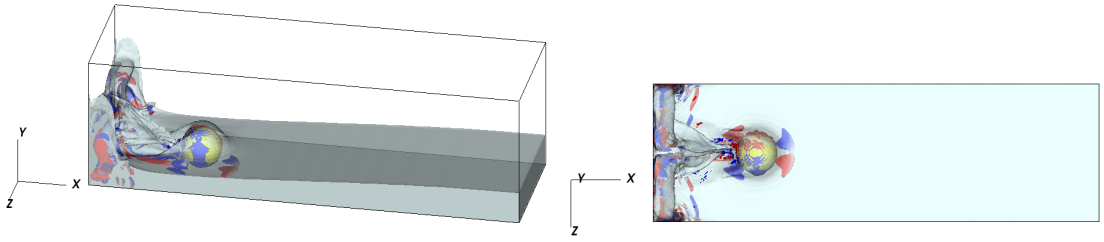

(c) t = 1.2 s

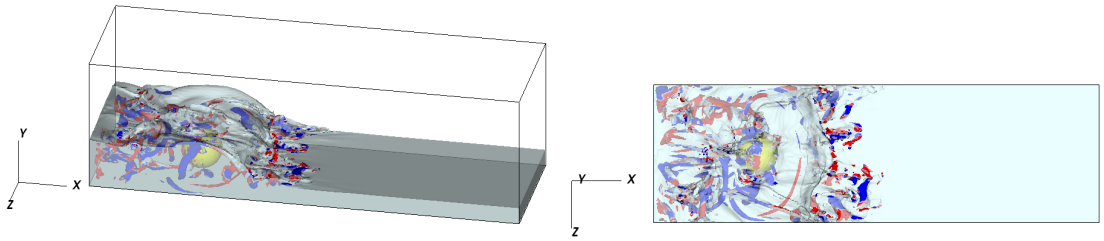

(d) t = 2.0 s

Fig. 7. Snapshots of the predicted water surface profile (shown as the isosurface of volume fraction F = 0.5) and turbulent vortical structure (colored by vertical vorticity component) at an oblique view (left panel) and top view (right panel) at t (s) = 0.56 (a), 0.8 (b), 1.2 (c), and 2.0 (d). Blue means negative vertical vorticity in which the flow moves clockwise and red means positive vertical vorticity in which the flow moves anti-clockwise.

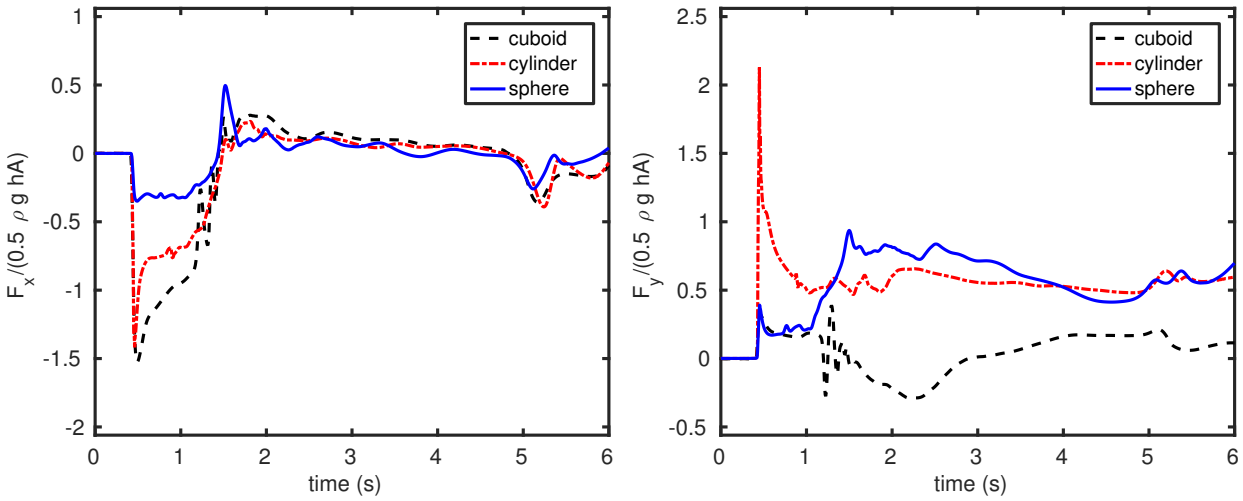

Fig. 8. Time history of the drag (a) and lift (b) force acting on the cuboid, cylinder and sphere during the dam-break flow. The force is normalised by $1/2\rho ghA$, where A is the cross section area.

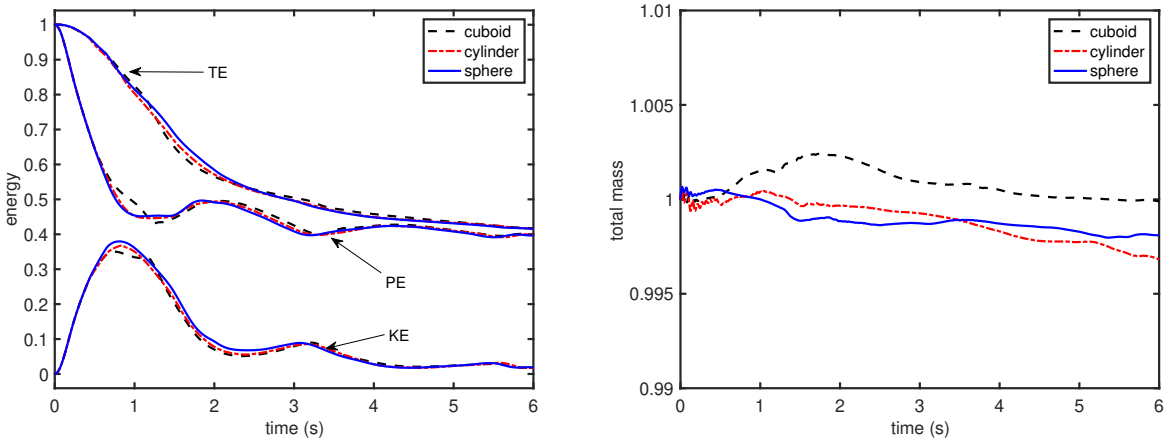

Fig. 9. Time history of the normalised energy (a) and total mass (b) during the dam-break flow over a cuboid, cylinder and sphere.